

Enhanced conductivity and weakened magnetism in Pb-doped Sr_2IrO_4

Zhi-Lai Yue(岳智来), Wei-Li Zhen(甄伟立), Rui Niu(牛瑞), Ke-Ke Jiao(焦珂珂), Wen-Ka Zhu(朱文卡), Li Pi(皮雳), and Chang-Jin Zhang(张昌锦)

Citation: Chin. Phys. B, 2024, 33 (**1**): 017402. DOI: 10.1088/1674-1056/ad08a9

Journal homepage: http://cpb.iphy.ac.cn; http://iopscience.iop.org/cpb

What follows is a list of articles you may be interested in

Rubidium-induced phase transitions among metallic, band-insulating, Mott-insulating phases in 1*T*-TaS_2

Zhengguo Wang(王政国), Weiliang Yao(姚伟良), Yudi Wang(王宇迪), Ziming Xin(信子鸣), Tingting Han(韩婷婷), Lei Chen(陈磊), Yi Ou(欧仪), Yu Zhu(朱玉), Cong Cai(蔡淙), Yuan Li(李源), and Yan Zhang(张焱)

Chin. Phys. B, 2023, 32 (**10**): 107404. DOI: 10.1088/1674-1056/acec40

Hole density dependent magnetic structure and anisotropy in Fe-pnictide superconductor

Yuan-Fang Yue(岳远放), Zhong-Bing Huang(黄忠兵), Huan Li(黎欢),Xing Ming(明 星), and Xiao-Jun Zheng(郑晓军)

Chin. Phys. B, 2023, 32 (**9**): 097403. DOI: 10.1088/1674-1056/acd328

Superconductivity and unconventional density waves in vanadium-based kagome materials AV_3Sb_5

Hui Chen(陈辉), Bin Hu(胡彬), Yuhan Ye(耶郁晗), Haitao Yang(杨海涛), and Hong-Jun Gao(高鸿钧)

Chin. Phys. B, 2022, 31 (**9**): 097405. DOI: 10.1088/1674-1056/ac7f95

Experimental observation of pseudogap in a modulation-doped Mott insulator: Sn/Si(111)-(√30×√30)*R*30°

Yan-Ling Xiong(熊艳翎), Jia-Qi Guan(关佳其), Rui-Feng Wang(汪瑞峰), Can-Li Song(宋灿立), Xu-Cun Ma(马旭村), and Qi-Kun Xue(薛其坤)

Chin. Phys. B, 2022, 31 (**6**): 067401. DOI: 10.1088/1674-1056/ac65f2

Pressure-induced anomalous insulating behavior in frustrated iridate $La_3Ir_3O_{11}$

Chun-Hua Chen(陈春华), Yong-Hui Zhou(周永惠), Ying Zhou(周颖), Yi-Fang Yuan(袁亦方), Chao An(安超), Xu-Liang Chen(陈绪亮), Zhao-Ming Tian(田召明), and Zhao-Rong Yang(杨昭荣)

Chin. Phys. B, 2021, 30 (**6**): 067402. DOI: 10.1088/1674-1056/abf100

Enhanced conductivity and weakened magnetism in Pb-doped Sr_2IrO_4

Zhi-Lai Yue(岳智来)[1,2], Wei-Li Zhen(甄伟立)[1], Rui Niu(牛瑞)[1], Ke-Ke Jiao(焦珂珂)[1], Wen-Ka Zhu(朱文卡)[1,†], Li Pi(皮雳)[1,2,‡], and Chang-Jin Zhang(张昌锦)[1,3,§]

[1] *High Magnetic Field Laboratory, Hefei Institutes of Physical Science, Chinese Academy of Sciences, Hefei* 230031, *China*
[2] *Science Island Branch of Graduate School, University of Science and Technology of China, Hefei* 230026, *China*
[3] *Collaborative Innovation Center of Advanced Microstructures, Nanjing University, Nanjing* 210093, *China*

(Received 20 September 2023; revised manuscript received 16 October 2023; accepted manuscript online 2 November 2023)

Group IV element Pb has been selected as the dopant to dope at the Sr site of Sr_2IrO_4. It is exciting to find that the single-phase crystal structure could be maintained with a high Pb doping level of up to $x = 0.3$ in $Sr_{2-x}Pb_xIrO_4$. The mapping data obtained from energy-dispersive x-ray spectroscopy analyses give solid evidence that the Pb ions are uniformly distributed in the Sr_2IrO_4 matrix. The incorporation of Pb leads to a moderate depression of the canted antiferromagnetic ordering state. The electrical conductivity could be greatly enhanced when the Pb doping content is higher than $x = 0.2$. The present results give a fresh material base to explore new physics in doped Sr_2IrO_4 systems.

Keywords: iridates, doping, conductivity, magnetism

PACS: 74.10.+v, 71.27.+a, 71.30.+h, 75.30.Kz **DOI:** 10.1088/1674-1056/ad08a9

1. Introduction

The search for possible room-temperature superconductors and the establishment of high-temperature superconducting mechanisms are two of the main scientific challenges facing the condensed matter physics community.[1] At ambient pressure, two classes of high-temperature superconducting materials, i.e., cuprate and iron-based superconductors,[2,3] have been discovered. The exploration of superconductors with transition temperature beyond the McMillan limit has attracted worldwide attention not only from the scientific community, but also from industry, as high-temperature superconductors have the potential to revolutionize electrical technology.[4] Besides the exploration of new superconducting materials, intensive experimental and theoretical investigations have been performed in order to unveil the mysterious pairing mechanisms of high-temperature superconductivity.[5–10] Despite the fact that significant progress has been achieved in the exploration of high-temperature superconducting mechanisms, the physical nature of the driving forces causing two electrons to form a superconducting pair is still under debate. Scientists are now eagerly expecting to discover a new family of high-temperature superconducting materials, which would greatly contribute to the final establishment of high-temperature superconducting mechanisms.

Sr_2IrO_4 is a 5d transition metal oxide material that has a similar layered perovskite-type crystal structure to the parent compound of the cuprate high-temperature superconductor, La_2CuO_4.[11] Similar to the $S = 1/2$ Mott insulating state in La_2CuO_4, the unique electronic and magnetic behaviors of Sr_2IrO_4 could be accounted by a novel $J_{\rm eff} = 1/2$ Mott insulating state due to large relativistic spin–orbit coupling.[12] This $J_{\rm eff} = 1/2$ Mott state leads to a canted antiferromagnetic ground state in Sr_2IrO_4, which is also reminiscent of the antiferromagnetic ground state in La_2CuO_4. Due to the similarities in the crystal structures and electronic and magnetic ground states of Sr_2IrO_4 and La_2CuO_4, it is natural to anticipate that similar physical phenomena, especially the possible high-temperature superconductivity, could be realized upon modulating the physical behaviors of Sr_2IrO_4 by chemical doping, pressure and other methods. Moreover, a series of theoretical work on the band structures and phase diagrams of doped Sr_2IrO_4 have predicted that possible high-temperature superconductivity could be achieved upon proper chemical doping.[13–16]

Experimentally, the effects of chemical doping on the Sr_2IrO_4 compound have been extensively investigated during the past several years.[17–28] Many intriguing physical phenomena, such as the formation of surface Fermi arcs and pseudogaps,[20] as well as the fragmented antiferromagnetic order,[22] have been observed. However, bulk superconductivity has not yet been achieved. Among the various possible dopants, La is the most often chosen element in investigations of the effects of doping on the physical properties of Sr_2IrO_4.[17,18,22,28] Generally, doping can result in structural

†Corresponding author. E-mail: wkzhu@hmfl.ac.cn
‡Corresponding author. E-mail: pili@ustc.edu.cn
§Corresponding author. E-mail: zhangcj@hmfl.ac.cn

© 2024 Chinese Physical Society and IOP Publishing Ltd

modifications of the parent material, which in turn leads to alterations of its band filling. In Sr_2IrO_4, partial substitution of Sr by La induces a change in the bandwidth.[17,18] However, the low solubility of dopants in Sr_2IrO_4 significantly limits the band filling control over a wide range. For instance, the transport data of a $(Sr_{1-x}La_x)_2IrO_4$ single crystal with $x = 0.04$ suggest that the insulating state could be driven into a metallic state.[29] However, no further data could be found with higher La doping level in Sr_2IrO_4 single crystals. Besides La, other rare-earth elements and metal elements, such as K, Tb, Nd, Pr and Nb, have been chosen as dopants to investigate the physical behaviors of doped Sr_2IrO_4.[23–27] It was quite surprising to find that the insulating state is very robust against doping in Sr_2IrO_4.[26] Thus it is necessary to extend the investigation of effects of doping in the Sr_2IrO_4 compound by choosing other possible elements as dopants.

In this work, we report the influence of Pb doping on the physical properties of Sr_2IrO_4. Pb is a group IV element which can be steadily coordinated at the A-site of ABO_3-type perovskite compounds such as $PbTiO_3$ and $Pb(Mg_{1/3}Nb_{2/3})O_3$.[30,31] Since Sr_2IrO_4 is crystallized in a K_2NiF_4-type perovskite structure where the coordination conditions of Sr-site ions are similar to those of A-site ions in ABO_3-type perovskite materials, we anticipate that Pb ions could be incorporated into the Sr site of Sr_2IrO_4. It is found that the solid solubility of Pb in $Sr_{2-x}Pb_xIrO_4$ could be as high as $x = 0.3$. The magnetic data reveal that although the long-range canted antiferromagnetic ordering state is substantially suppressed by Pb doping, the net ferromagnetic moment could still be detected even in the $x = 0.3$ sample. Quantitatively, the net ferromagnetic moment decreases from 0.042 μ_B/Ir in the parent Sr_2IrO_4 sample to 0.033 μ_B/Ir in the $x = 0.3$ sample. Compared to those reported in previous literatures, the suppression of magnetic ordering state in Pb-doped samples is the weakest among the doped Sr_2IrO_4 compounds, suggesting that Pb ions do not severely alter the pristine ordered magnetic state in the Sr_2IrO_4 system. The $Sr_{2-x}Pb_xIrO_4$ polycrystalline samples exhibit an insulator-like behavior when the Pb doping content is less than $x = 0.2$. When the Pb doping level is higher than 0.2, a drastic increase of conductivity is seen, particularly in the low-temperature region. The greatly enhanced conductivity in $Sr_{2-x}Pb_xIrO_4$ polycrystalline samples deserves further study through subsequent single-crystal growth and a comprehensive investigation of their physical properties. Taking into account the high solid solubility of Pb in the Sr_2IrO_4 matrix, $Sr_{2-x}Pb_xIrO_4$ compounds could serve as ideal material bases in future investigations of doping-induced physical phenomena in the Sr_2IrO_4 system.

2. Experiment

The $Sr_{2-x}Pb_xIrO_4$ polycrystalline samples were prepared via a conventional solid-state reaction technique. In detail, mixtures of high purity Sr_2CO_3, PbO and IrO_2 were weighed at a stoichiometric molar ratio of $SrCO_3$:PbO:$IrO_2 = (2-x) : x : 1.02$ and thoroughly mixed in an agate mortar. In order to compensate for the possible loss of Ir at high temperature, we added 2% of additional IrO_2 in the starting materials. The mixtures were loaded into alumina crucibles and put into a high-temperature furnace, which was preheated to 1100 °C for 24 hours. After another grinding, the mixtures were re-heated once again at 1150 °C for 24 hours. Then the mixtures were ground and pressed into pellets. The pellets were finally sintered at 1150 °C for 48 hours.

Powder x-ray diffraction (XRD) data were collected by a PANalytical X'Pert Pro MPD detector using monochromated Cu $K_{\alpha 1}$ radiation as the x-ray source. The chemical compositions of the samples were determined with the aim of energy dispersive x-ray spectrometry analyses using an Oxford Swift 3000 spectrometer equipped with a Hitachi TM3000 scanning electron microscope. The temperature and field dependences of magnetization were measured on a Quantum Design superconducting quantum interference device magnetometer. The temperature dependence of resistivity was measured on a physical property measurement system using the standard four-probe method.

3. Results and discussion

Figure 1(a) shows the powder XRD patterns of the $Sr_{2-x}Pb_xIrO_4$ samples. The parent material of Sr_2IrO_4 crystallizes in a K_2NiF_4-type perovskite tetrahedral-phase structure, with space group $I4_1/acd$.[11] It can be seen from Fig. 1(a) that all the XRD diffraction peaks of the $Sr_{2-x}Pb_xIrO_4$ samples are nearly identical to those of the Sr_2IrO_4 parent sample, without any impurity peaks. This fact suggests that all $Sr_{2-x}Pb_xIrO_4$ samples are crystallized into a single-phase crystal structure. In order to quantitatively determine the lattice parameters of the $Sr_{2-x}Pb_xIrO_4$ samples, we performed detailed Rietveld refinements on the XRD data. Typical Rietveld refinement results of the $x = 0.3$ sample are shown in Fig. 1(b). It can be seen that the calculated curve can well reproduce the experimental data, suggesting that the refinements are reliable. Figure 1(c) gives the variations of the a- and c-axis lattice constants of the $Sr_{2-x}Pb_xIrO_4$ samples. The a- and c-axis lattice constants of the undoped Sr_2IrO_4 sample are 5.4905 Å and 25.751 Å, respectively. These values are consistent with those reported in the literature.[11] With increasing Pb doping, both a- and c-axis lattice constants increase monotonously, reflecting the influence of Pb dopants on the lattice structures.

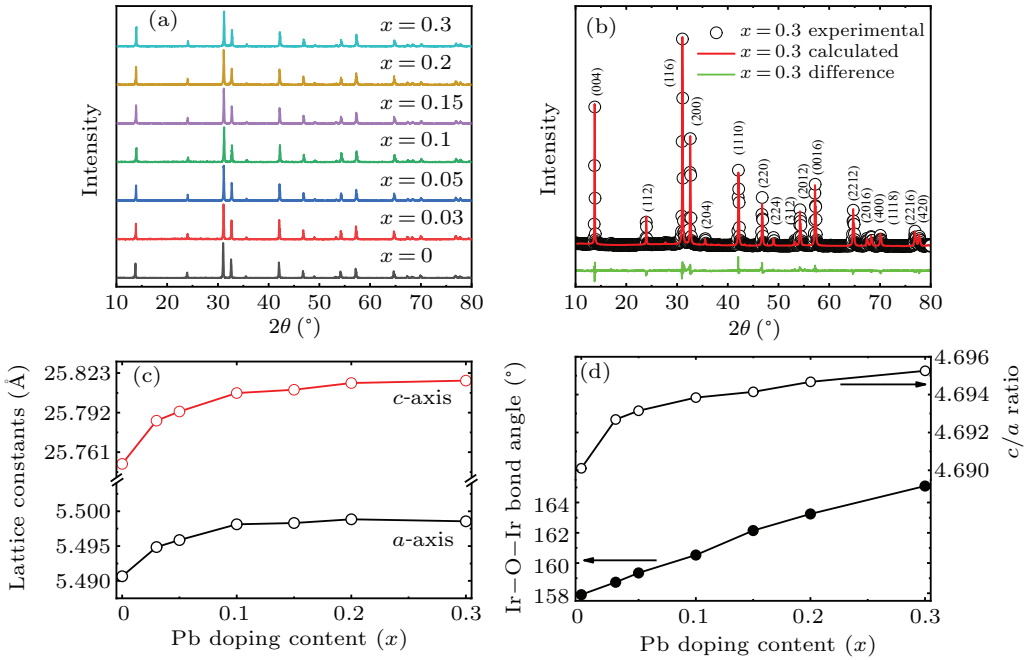


Fig. 1. (a) Powder XRD patterns of the $Sr_{2-x}Pb_xIrO_4$ samples detected at room temperature. (b) Typical Rietveld refinements to the $x = 0.3$ sample. The black hollow circles are experimental data. The red curve is the fitting to experimental data. The green curve is the difference between the experimental data and the fitting results. (c) The variations of lattice constants with increasing Pb doping. (d) The lattice constant ratio of the c- to a-axis (c/a ratio) and the in-plane Ir–O–Ir bond angle at different Pb doping levels.

It is well known that the IrO_6 octahedra in Sr_2IrO_4 are rotated around the crystallographic c axis by about 11°.[11] As a consequence of this rotation, the in-plane Ir–O–Ir bond is significantly bent away from a perfect IrO_2 plane. The resultant in-plane Ir–O–Ir bond angle is about 157.9° in the pristine Sr_2IrO_4 sample. It is not yet clear whether or not the bent character of the Ir–O–Ir bond plays a crucial role in determining the transport and magnetic properties of the Sr_2IrO_4 compound. In order to learn the influence of Pb doping on the Ir–O–Ir bond of the $Sr_{2-x}Pb_xIrO_4$ samples, we calculated the in-plane Ir–O–Ir bond angle of the Pb-doped samples. The results are plotted in Fig. 1(d). It can be seen that the introduction of Pb results in a monotonous increase of the in-plane Ir–O–Ir bond angle. The monotonous strengthening of the in-plane Ir–O–Ir bond indicates that the rotation of IrO_6 octahedra is substantially released in Pb-doped samples. In Fig. 1(d) we give the lattice constant ratio of the c- to the a-axis (c/a ratio) at different Pb doping levels. It is found that the c/a ratio monotonously increases with increasing Pb doping. In a layered perovskite oxide, the enhanced c/a ratio suggests that the material becomes more two-dimensional. This two-dimensional feature is consistent with the increased Ir–O–Ir bond angle.

In order to know whether or not the Pb ions are uniformly distributed and to what extent the Pb ions are melted into the samples, we performed energy dispersive x-ray spectrometry (EDX) analyses on the $Sr_{2-x}Pb_xIrO_4$ samples. Figure 2 shows the typical EDX spectrum of the $x = 0.3$ sample. It can be seen from the elemental mapping data of Figs. 2(a)–2(c) that the Sr, Pb and Ir ions are all nearly uniformly distributed in the $Sr_{2-x}Pb_xIrO_4$ polycrystalline samples, with no evidence of phase separations. The distribution of Pb is regular, confirming the successful incorporation of Pb in the Sr_2IrO_4 matrix. Figure 2(d) gives a typical EDS spectrum of the $x = 0.3$ sample. The quantitative analyses of the EDS spectra of the $Sr_{2-x}Pb_xIrO_4$ samples confirm that the real compositions of the obtained samples are comparable to the nominal compositions. Combining the XRD data and the EDS results, it is suggested that the Pb ions are uniformly incorporated into the Sr_2IrO_4 matrix, with solid solubility as high as $x = 0.3$.

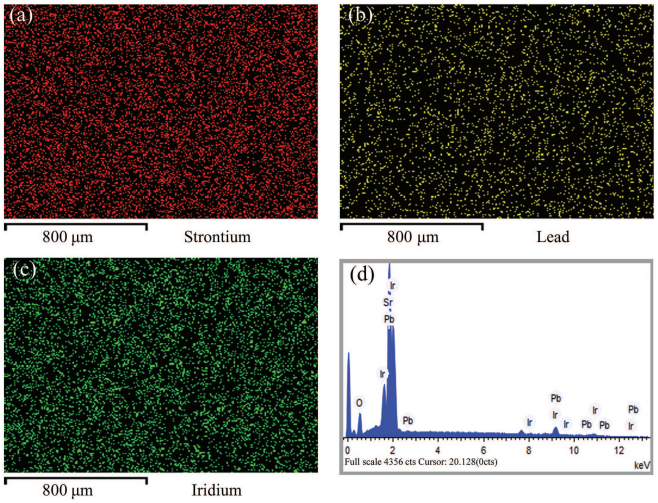


Fig. 2. (a)–(c) The energy-dispersive x-ray spectroscopy (EDS) mapping data of the Sr (a), Pb (b) and Ir (c) elements of the $Sr_{1.7}Pb_{0.3}IrO_4$ sample. (d) A typical EDS spectrum confirming the chemical composition of $Sr_{1.7}Pb_{0.3}IrO_4$.

Figure 3(a) gives the temperature dependence of dc mag-

netic susceptibility (χ–T) of the $Sr_{2-x}Pb_xIrO_4$ samples measured under zero-field-cooling (ZFC) and field-cooling (FC) processes. For the parent Sr_2IrO_4 sample, the χ–T curves exhibit a paramagnetic-like behavior at high temperature, with the χ–T curves measured under the ZFC and FC conditions nearly identical. Below $T_N \sim 240$ K, the χ–T curves exhibit a drastic upturn with decreasing temperature. In addition, the χ–T curves measured under ZFC condition and FC condition diverge, consistent with the formation of a canted antiferromagnetic state.[12] Previous studies have revealed that the Ir 5d orbitals are strongly hybridized with the neighboring O 2p orbitals and thus significant parts of the moments are canceled in the canted antiferromagnetic ordered state, leading to a net ferromagnetism in Sr_2IrO_4.[11,12]

A remarkable observation is that the Néel temperature T_N stays at about 240 K in all Pb-doped samples. The nearly unchanged Néel temperature in the Pb-doped samples is sharply different from that in many other elements (such as La, K, Tb, Sm, Pr, and Nb) doped samples, where the incorporation of dopants readily depresses the antiferromagnetic ordering state.[17,21–26] Interestingly, we find that the nearly unchanged T_N hints at a certain similarity to the cases in Fe and Sc doping at the Ir-site of Sr_2IrO_4.[32,33] In Fe-doped samples, it is suggested that the Fe dopants have only a $S = 1$ spin, thus carrying very small magnetic moments that are too weak to effectively affect the superexchange interactions between the Ir ions.[32] In the Pb-doped samples, the charge-transfer effect between the Sr(Pb)O layer and the IrO_2 layer is weak; thus the superexchange interactions within the InO_2 layer is hardly influenced.

It should be noted that with the incorporation of Pb, the absolute value of magnetic susceptibility exhibits a slight decrease. The decrease of the absolute value of magnetic susceptibility means that the net ferromagnetic moment is slightly decreased in the Pb-doped samples. Figure 3(b) gives the irreversibility curve of the $Sr_{2-x}Pb_xIrO_4$ samples obtained by subtracting the ZFC data from the FC data. It can be seen that the amplitude of the irreversibility data decreases with increasing Pb doping content, consistent with the decrease of net ferromagnetic moment. The decrease of net ferromagnetic moment is due to the strong coupling of the magnetic moment and lattice.[34–36] Due to the coupling of the magnetic moment and lattice, a relaxed Ir–O–Ir bond angle (Fig. 1(c)) inevitably weakens the Dzyaloshinskii–Moriya interaction that drives the canted antiferromagnetic ordering state in Sr_2IrO_4, leading to the decrease of net ferromagnetic moment. It can be also seen from Fig. 3(b) that the decrease of net ferromagnetic moment is small in all Pb-doped samples. Quantitatively, the net ferromagnetic moment decreases from 0.042 μ_B/Ir in the undoped Sr_2IrO_4 sample to 0.033 μ_B/Ir in the $x = 0.3$ sample. This small decrease of net ferromagnetic moment suggests that the introduction of Pb dopants only moderately suppresses its magnetic ordered state. Figure 3(c) gives the isothermal magnetization (M–H) curve of the $x = 0.3$ sample. The apparent magnetic hysteresis loop displayed in the M–H curve of the $x = 0.3$ sample confirms that a substantial amount of net ferromagnetic moment still survives in heavily Pb-doped samples.

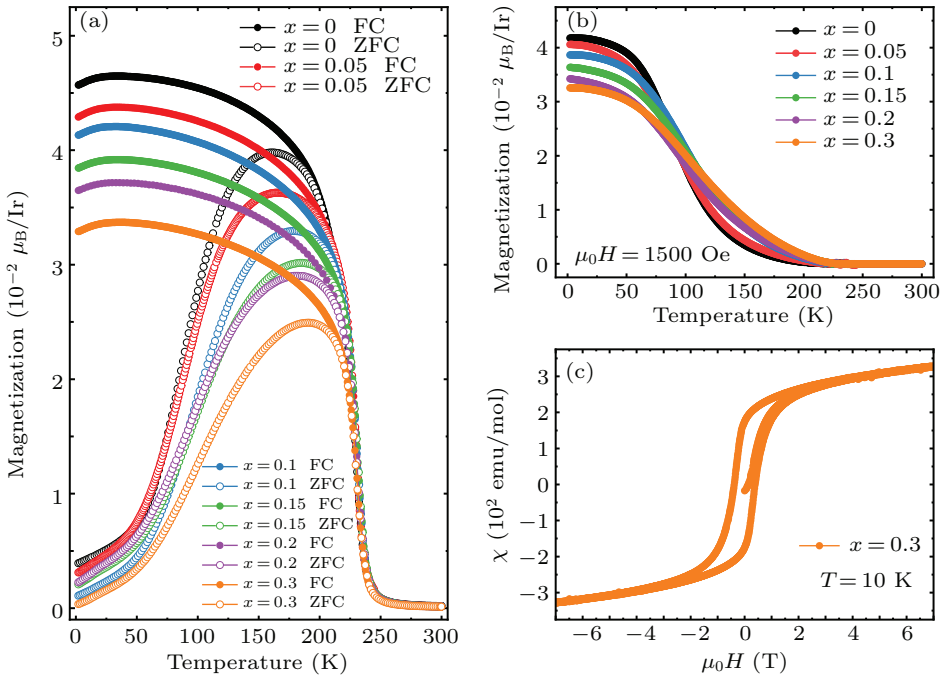


Fig. 3. (a) Temperature dependence of DC magnetic susceptibility of the $Sr_{2-x}Pb_xIrO_4$ samples measured under zero-field-cooling (ZFC) and field-cooling (FC) processes. The applied magnetic field is 1500 Oe. (b) The irreversibility curve of the DC magnetic susceptibility of the $Sr_{2-x}Pb_xIrO_4$ samples obtained by subtracting the ZFC data from the FC data. (c) Magnetic field dependence of DC magnetization of the $x = 0.3$ sample measured at 10 K.

Figure 4(a) shows the temperature dependence of resistivity (ρ–T) of the $Sr_{2-x}Pb_xIrO_4$ samples. The undoped Sr_2IrO_4 sample exhibits a typical insulator-like behavior over the whole temperature range, consistent with its spin–orbit coupling driven $J_{\rm eff} = 1/2$ Mott insulating state.[12] With the incorporation of Pb, the resistivity decreases in the 100 K–300 K temperature region, suggesting an enhanced conductivity. For the $x \leq 0.15$ samples, they exhibit typical insulator-like behavior over the whole temperature range, similar to the undoped Sr_2IrO_4 sample. However, for the $x \geq 0.2$ samples, the ρ–T curves exhibit different features compared to those of the $x \leq 0.15$ samples. For example, the resistivity only displays a small increase with decreasing temperature, showing typical semiconductor-like behavior. In addition, there is an inflection point at around 100 K. These different features suggest that the incorporation of a sufficient amount of Pb could alter the electronic conductivity of the $Sr_{2-x}Pb_xIrO_4$ compounds.

In order to learn more about the conductive mechanisms of the $Sr_{2-x}Pb_xIrO_4$ samples, we perform a fitting to the ρ–T curves of the samples. The fitting is performed according to the segmentation fitting method proposed by Kini *et al.*[37] In the high temperature region (210 K–300 K), the ρ–T curves of Sr_2IrO_4 could be fitted using the logarithmic relation of $\rho(T) = \rho_0 e^{-\alpha T}$, where ρ_0 and α are constants dependent on the samples. The $\ln\rho$–T curves of the $Sr_{2-x}Pb_xIrO_4$ samples are plotted in Fig. 4(b). It can be seen that the $\ln\rho$–T curves of all $Sr_{2-x}Pb_xIrO_4$ samples yield nearly linear behavior in the 210 K–300 K regions, suggesting that the logarithmic relation could well explain the transport mechanisms of the $Sr_{2-x}Pb_xIrO_4$ samples. In the intermediate temperature region of 110 K–190 K, Kini *et al.* suggest that the conduction mechanism of Sr_2IrO_4 could be described using a thermally activated model according to an Arrhenius type relation of $\rho(T) = \rho_0 e^{\Delta/(2k_BT)}$, where Δ is a constant relating to the energy gap of the sample and k_B is the Boltzmann constant. The nearly linear $\ln\rho$–T^{-1} curves displayed in Fig. 4(c) suggest that the conduction mechanism of the $Sr_{2-x}Pb_xIrO_4$ samples could be ascribed using the thermally activated model in the 110 K–190 K temperature region. According to the slope of the $\ln\rho$–T^{-1} curves, the energy gap of the $Sr_{2-x}Pb_xIrO_4$ samples can be derived. The energy gap of the Sr_2IrO_4 sample is 115 meV, which is consistent with the small theoretically calculated gap value.[38] The energy gap decreases monotonously with increasing Pb doping. For example, the energy gaps of the $x = 0.1$ and 0.2 samples are 104 meV and 38 meV, respectively. For the $x = 0.3$ sample, the energy gap is only 4.1 meV. The continuous decrease of energy gap could be connected to the increase of Ir–O–Ir bond angle with Pb doping. In Sr_2IrO_4, the significantly bent Ir–O–Ir bond hinders the free motion of charge carriers within the IrO_2 conductive plane. With the incorporation of Pb, the in-plane Ir–O–Ir bond becomes straightened. The straightened Ir–O–Ir bond favors orbital hybridization between the Ir 4f electrons and the O 2p electrons, leading to a monotonous decrease of the energy gap and an enhancement of the electrical conductivity in $Sr_{2-x}Pb_xIrO_4$ samples.

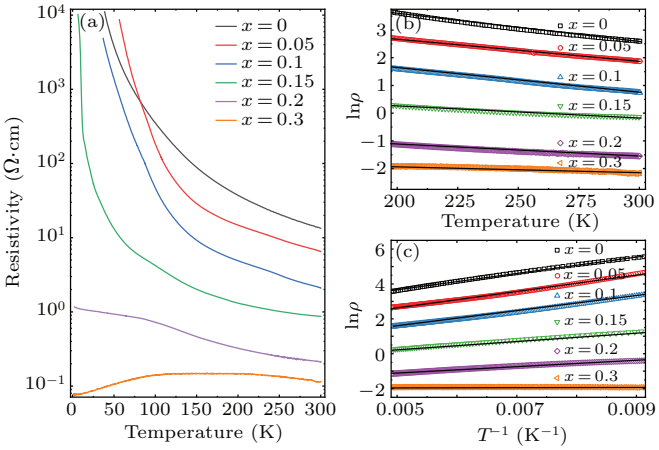


Fig. 4. (a) Temperature dependence of resistivity of the $Sr_{2-x}Pb_xIrO_4$ polycrystalline samples. (b) The $\ln\rho$ versus T curves in the 210–300 K temperature region. (c) The $\ln\rho$ versus T^{-1} curves in the 110–190 K temperature region.

4. Conclusion

We report the synthesis and physical properties of a series of $Sr_{2-x}Pb_xIrO_4$ samples. The detailed Rietveld refinements to the x-ray diffraction data and the energy-dispersive x-ray spectrometry analyses provide dual evidence that the Pb ions are successfully incorporated into the Sr_2IrO_4 matrix with solid solubility up to $x = 0.3$. The incorporation of Pb results in a moderate destruction of the canted antiferromagnetic state of the Sr_2IrO_4 compound. The incorporation of Pb substantially enhances the conductivity of $Sr_{2-x}Pb_xIrO_4$ samples at high temperature. The energy gap decreases monotonously with increased Pb doping. However, the energy gap could not reach zero even in the heaviest Pb-doped samples. Despite the greatly enhanced conductivity, complete metallization remains unrealized in $Sr_{2-x}Pb_xIrO_4$ samples. In future, the growth of single crystals and the investigation of the physical properties of $Sr_{2-x}Pb_xIrO_4$ single-crystal samples are needed. In addition, preparing the Pb-doped samples with $x > 0.3$ using unconventional synthetic techniques such as the high-pressure high-temperature method is highly anticipated in order to realize complete metallization and, more importantly, superconductivity.

Acknowledgements

Project supported by the National Key R&D Program of China (Grant Nos. 2022YFA1403203 and 2021YFA1600201), the National Natural Science Foundation of China (Grant Nos. 11974356 and 12274414), the Joint Funds of the National Natural Science Foundation of China and the Chinese

Academy of Sciences Large-Scale Scientific Facility (Grant No. U1932216).

References

[1] Hussey N E and Duffy C 2022 *Sci. Bull.* **67** 985
[2] Bednorz J G and Müller K A 1986 *Z. Phys. B* **64** 189
[3] Kamihara Y, Watanabe T, Hirano M and Hosono H 2008 *J. Am. Chem. Soc.* **130** 3296
[4] Kaur H, Kaur H and Sharma A 2021 *Mater. Today-Proc.* **37** 3612
[5] Tsuei C C and Kirtley J R 2000 *Rev. Mod. Phys.* **72** 969
[6] Keimer B, Kivelson S A, Norman M R, Uchida S and Zaanen J 2015 *Nature* **518** 179
[7] Hussey N E, Buhot J and Licciardello S 2018 *Rep. Prog. Phys.* **81** 052501
[8] Sobirey L, Luick N, Bohlen M, Biss H, Moritz H and Lompe T 2021 *Science* **372** 844
[9] Zhao J Y and Weng Z Y 2022 *Chin. Phys. B* **31** 087104
[10] El Hage R, Humbert V, Rouco V, Sanchez-Santolino G, Lagarrigue A, Seurre K, Carreira S J, Sander A, Charliac J, Mesoraca S, Trastoy J, Briatico J, Santamaria J and Villegas J E 2023 *Nat. Commun.* **14** 3010
[11] Crawford M K, Subramanian M A, Harlow R L, Fernandez-Baca J A, Wang Z R and Johnston D C 1994 *Phys. Rev. B* **49** 9198
[12] Kim B J, Jin H, Moon S J, Kim J Y, Park B G, Leem C S, Yu J, Noh T W, Kim C, Oh S J, Park J H, Durairaj V, Cao G and Rotenberg E 2008 *Phys. Rev. Lett.* **101** 076402
[13] Wang F and Senthil T 2011 *Phys. Rev. Lett.* **106** 136402
[14] Watanabe H, Shirakawa T and Yunoki S 2013 *Phys. Rev. Lett.* **110** 027002
[15] Kang J and Yuan Y H 2020 *Physica C* **572** 1353621
[16] Peng S T, Lane C, Hu Y, Guo M Y, Chen X, Sun Z L, Hashimoto M, Lu D H, Shen Z X, Wu T, Chen X H, Markiewicz R S, Wang Y, Bansil A, Wilson S D and He J F 2022 *npj Quant. Mater.* **7** 58
[17] Chen X, Hogan T, Walkup D, Zhou W W, Pokharel M, Yao M L, Tian W, Ward T Z, Zhao Y, Parshall D, Opeil C, Lynn J W, Madhavan V and Wilson S D 2015 *Phys. Rev. B* **92** 075125
[18] Brouet V, Mansart J, Perfetti L, Piovera C, Vobornik I, Le Fevre P, Bertran F, Riggs S C, Shapiro M C, Giraldo-Gallo P and Fisher I R 2015 *Phys. Rev. B* **92** 081117
[19] Yan Y J, Ren M Q, Xu H C, Xie B P, Tao R, Choi H Y, Lee N, Choi Y J, Zhang T and Feng D L 2015 *Phys. Rev. X* **5** 041018
[20] Kim Y K, Sung N H, Denlinger J D and Kim B J 2016 *Nat. Phys.* **12** 37
[21] Horigane K, Fujii M, Okabe H, Kobayashi K, Horie R, Ishii H, Liao Y F, Kubozono Y, Koda A, Kadono R and Akimitsu J 2018 *Phys. Rev. B* **97** 064425
[22] Zhao H, Manna S, Porter Z, Chen X, Uzdejczyk A, Moodera J, Wang Z Q, Wilson S D and Zeljkovic I 2019 *Nat. Phys.* **15** 1267
[23] Nelson J N, Parzyck C T, Faeth B D, Kawasaki J K, Schlom D G and Shen K M 2020 *Nat. Commun.* **11** 2597
[24] Huang H, Ji P, Xie Y, Han H and Ge B H 2020 *Phys. Rev. Mater.* **4** 115001
[25] Kim S W, Kang M and Cheon S 2021 *Phys. Rev. B* **103** 045116
[26] Huang H, Ji P, Han H, Duan H M, Ling L H and Ge B H 2022 *J. Supercond. Novel Magn.* **35** 733
[27] Yang J F, Guo W, Xu Z H, Liu Y W, Sun H Y, Sun W J, Yan S J, Li Y Y, Gu Z B, Zhou J, Zhu Y and Nie Y F 2023 *Phys. Rev. B* **107** 235152
[28] Liu M R, Yue J N, Meng J C, Shao T N, Yao C L, Sun X J, Nie J C and Li D B 2023 *Appl. Phys. Lett.* **122** 022402
[29] Ge M, Qi T F, Korneta O B, De Long D E, Schlottmann P, Crummett W P and Cao G 2011 *Phys. Rev. B* **84** 100402
[30] Rizwan S, Zhang S, Yu T, Zhao Y, Zhang S and Han X 2011 *Chin. Phys. Lett.* **28** 107308
[31] Windsor D and Xu H 2023 *Phys. Rev. Mater.* **7** 055004
[32] Hu B, Zhao H D, Zhang Y, Schlottmann P, Ye F and Cao G 2021 *Phys. Rev. B* **103** 115122
[33] Huang H, Wang C F, He X J, Zu H, Ji P and Duan H M 2023 *Physica B* **665** 415045
[34] Torchinsky D H, Chu H, Zhao L, Perkins N B, Sizyuk Y, Qi T, Cao G and Hsieh D 2015 *Phys. Rev. Lett.* **114** 096404
[35] Cao G and Schlottmann P 2018 *Rep. Prog. Phys.* **81** 042502
[36] Engström L, Pereg-Barnea T and Witczak-Krempa W 2021 *Phys. Rev. B* **103** 155147
[37] Kini N, Strydom A M, Jeevan H S, Geibel C and Ramakrishnan S 2006 *J. Phys.: Condens. Matter* **18** 8205
[38] Lane C, Zhang Y B, Furness J W, Markiewicz R S, Barbiellini B, Sun J W and Bansil A 2020 *Phys. Rev. B* **101** 155110